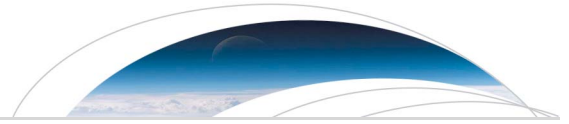




Originally published as:

Shahraki, M., Schmeling, H., Kaban, M. K., Petrunin, A. G. (2015): Effects of the postperovskite phase change on the observed geoid. - *Geophysical Research Letters*, 42, 1, p. 44-52.

DOI: <http://doi.org/10.1002/2014GL060255>



RESEARCH LETTER

10.1002/2014GL060255

Key Points:

- Geoid anomalies are strongly affected by the presence of pPv
- While geoid increased for the high viscous pPv, the weak pPv reduces the geoid
- Robustness tests with different parameters were performed, and the result noted

Supporting Information:

- Readme
- Figure S1
- Figure S2
- Figure S3
- Figure S4
- Figure S5
- Figure S6
- Figure S7
- Table S1
- Data Set S1

Correspondence to:

M. Shahraki,
Shahraki@geophysik-uni-frankfurt.de

Citation:

Shahraki, M., H. Schmeling, M. K. Kaban, and A. G. Petrunin (2015), Effects of the postperovskite phase change on the observed geoid, *Geophys. Res. Lett.*, *42*, 44–52, doi:10.1002/2014GL060255.

Received 21 OCT 2014

Accepted 9 DEC 2014

Accepted article online 12 DEC 2014

Published online 6 JAN 2015

Effects of the postperovskite phase change on the observed geoid

M. Shahraki¹, H. Schmeling¹, M. K. Kaban², and A. G. Petrunin²

¹Institut für Geowissenschaften, Fachinheit Geophysik, Goethe Universität, Frankfurt am Main, Germany, ²Helmholtz Center Potsdam, GFZ German Research Center for Geosciences, Potsdam, Germany

Abstract In the lowermost mantle, seismic velocity variations beneath Pacific margins have been related to the perovskite to postperovskite (pPv) phase transition. We investigate the influence of this phase transformation on the geoid using 3-D spherical mantle circulation models based on a seismic tomography model and strong lateral viscosity variations in the lower mantle. We demonstrate that the geoid anomalies are strongly affected by the presence of pPv because of phase-dependent viscosity changes relative to the surrounding mantle. Whereas geoid heights above subduction zones are increased for high-viscosity pPv, the presence of weak pPv reduces them, thereby improving the fit to the observed geoid. An investigation using two different tomography models, different pPv density contrasts, and the presence or absence of a global thermal boundary layer and of lateral viscosity variations in the lower mantle demonstrates the various effects of weak pPv on the geoid.

1. Introduction

The discovery of the phase transition in Mg-perovskite to the high-pressure postperovskite phase at the core-mantle boundary (CMB) has had a great influence on our understanding of the nature of the D'' region of the lowermost mantle. Direct evidence for the phase transition from perovskite (pv) to postperovskite (pPv) has been obtained using both experimental and theoretical techniques [Murakami *et al.*, 2004; Oganov and Ono, 2004; Shim *et al.*, 2004; Tsuchiya *et al.*, 2004]; in addition, indirect evidence of this transition has been provided based on the seismic anisotropy in the lower mantle [e.g., Hernlund, 2013; Nowacki *et al.*, 2010]. As an exothermic phase transition, cold downwelling material such as slabs may experience this phase transformation close to the CMB, whereas hot regions are expected to remain in the pv phase.

The electrical conductivity of pPv has been determined to be several orders of magnitude greater than that of pv [Ohta *et al.*, 2008], indicating a strong heterogeneity in the lowermost mantle. Nevertheless, the magnitude and even the sign of the viscosity contrast remain disputed. Although most studies support the concept of a weak pPv [Ammann *et al.*, 2010; Hunt *et al.*, 2009], other studies have argued for the possibility of a stronger viscosity in the pPv region [Karato, 2011].

The physical properties of pPv are still being explored. Ammann *et al.* [2010] showed that diffusion in pPv is highly anisotropic (approximately 8 orders of magnitude) and that diffusion creep is controlled by the slowest diffusion direction, whereas dislocation creep is controlled by the fastest diffusion direction. Accordingly, these authors concluded that the pPv viscosity can be 2 to 3 orders of magnitude lower than the pv viscosity. However, Karato [2010] suggested that dislocation creep could be controlled by the direction in which the diffusion coefficient is intermediate. Moreover, he argued that additional information is needed to constrain the magnitude of the diffusion coefficients and creep behavior of the pPv mineral.

Recent studies of the pPv phase change have determined that the pPv rheology has a first-order influence on the mantle dynamics [Cizkova *et al.*, 2010; Nakagawa and Tackley, 2011]. Therefore, it is reasonable to use the observed geoid and dynamic topography to constrain the lateral viscosity variations (LVVs) in the D'' layer.

Geoid variations have been used to infer radial viscosity [Kido and Cadek, 1997; Ricard *et al.*, 1984; Richards and Hager, 1984] and the possible effects of LVVs [Cadek and Fleitout, 2003; Kaban *et al.*, 2007; Richards and Hager, 1989; Zhang and Christensen, 1993; Zhong and Davies, 1999]. Although a conclusive agreement has not been reached regarding the sensitivity of the geoid to LVVs, these lateral variations might be important, particularly if they are located in boundary layers [Cadek and Fleitout, 2006] and as weak zones along plate boundaries [Kaban *et al.*, 2014]. The results of studies concerning the effects of LVVs on the geoid due to

the presence of the pv-pV phase transition have been ambiguous. Certain studies found a significant effect [Tosi *et al.*, 2009a, 2009b], whereas others indicated that LVVs above the CMB in combination with stiff lower mantle slabs have little influence on the geoid compared with the radial viscosity variations [e.g., Ghosh *et al.*, 2010].

Recently, Tosi *et al.* [2009b] performed a parametric study regarding the effect of pPv on the long-wavelength geoid. However, their results were limited to a 2-D axisymmetric geometry with a simplified density and viscosity structure, and the conclusions regarding the effects of LVVs may vary when considering the actual 3-D density and viscosity structure of the mantle. This variation might be especially important if the LVVs are located in the top and bottom thermal boundary layers [Cadek and Fleitout, 2003, 2006]. Moreover, a 2-D model cannot describe the excitation of toroidal flow and its coupling with poloidal flows [e.g., Moucha *et al.*, 2007]. Thus, the investigation of LVV effects requires the construction of a mantle flow model having a fully 3-D spherical geometry.

In a pioneering study, Cadek and Fleitout [2006] considered LVVs in the D'' layer while omitting LVVs in the mantle. They suggested that LVVs above the CMB may significantly influence the gravitational field compared with a radial viscosity distribution alone. Nevertheless, the consideration of LVVs in the D'' layer together with highly viscous slabs in the lower mantle may modify the influence of LVVs on the long-wavelength geoid.

More recently, Ghosh *et al.* [2010] used the slab model LRR98D [Ricard *et al.*, 1993] and introduced a low-viscosity region beneath the slab that can be considered as the pPv zone in the lowermost mantle [Hunt *et al.*, 2009]. For a specific configuration, they found that the geoid fit was degraded with the presence of LVVs in the lower mantle. However, they showed that assuming pPv regions with 3 orders of magnitude smaller viscosity, the geoid fit can be recovered. Thus, the presence of weak pPv could counteract the effects of stiff slabs, leading to a global correlation similar to that occurring without LVV (radial case).

The above findings suggest that a parameter study using recent seismic tomography data is needed to investigate the presence of pPv in the D'' layer that can incorporate large LVVs into the overlying mantle. The aim of the present study was to perform such a parameter space study using a 3-D spherical model.

As the objective of this study was to understand the specific effect of the presence of pPv in the D'' layer, we did not adjust the predicted geoid to the observed geoid to obtain the best possible fit by tuning various radial viscosity parameters. Thus, the relative variations due to pPv-related LVVs should be more meaningful than the absolute fit.

2. Method and Model

To evaluate the effect of postperovskite in the lowermost mantle on the dynamic topography and geoid heights, we performed numerical simulations with a 3-D spherical model using the Boussinesq approximation with an infinite Prandtl number. We solved the equations of mass and momentum conservation using the Ying-Yang grid system [e.g., Yoshida and Kageyama, 2004] and a staggered-grid, finite-volume method [Yoshida, 2008].

The nondimensional equations governing the instantaneous mantle flow with spatially variable viscosity take the following form:

$$\nabla \cdot v = 0 \quad (1)$$

$$-\nabla p + \nabla \cdot \{ \eta (\nabla v + \nabla v^{\text{tr}}) \} - Ra_{sc} \delta \rho e_r = 0 \quad (2)$$

where v is the velocity vector, p is the dynamic pressure, η is the viscosity, $\delta \rho$ is the nondimensional density anomaly, e_r is the unit vector in radial direction, and superscript tr indicates the tensor transpose. The scaling Rayleigh number Ra_{sc} is given by the following:

$$Ra_{sc} = \frac{\rho_0 g b^3}{\kappa_0 \eta_0} \quad (3)$$

where ρ_0 is the reference density, g is the gravitational acceleration, b is the thickness of the mantle layer, κ_0 is the reference thermal diffusivity, and η_0 is the reference viscosity. The scaling Rayleigh number is related to Rayleigh number (Ra) by $Ra = Ra_{sc} \times \alpha \Delta T$, where α and ΔT are the thermal expansivity and scaling temperature, respectively (see Table S1 in the supporting information).

The size of the computational grid is 100 (in radial) \times 180 (in latitudinal) \times 540 (in longitudinal) \times 2 (Yin-Yang grids), and we performed a resolution test at both higher and lower resolutions to ensure that our results are adequately resolved and numerically stable. Impermeable and shear stress-free conditions are adopted at both the top and bottom surface boundaries.

To calculate the gravitational response of a dynamic mantle, the matrix propagator method can be employed to simultaneously solve Poisson's equation with the equations governing the viscous flow induced by density anomalies in the mantle, as described above [e.g., *Hager and Clayton*, 1989]. However, in the presence of lateral viscosity variation, this method is no longer applicable, and a finite volume method with spectral decomposition of density and topography is required allowing to solve the gravitational potential equation in the spectral domain. Here we used this technique, which is presented in *Shahraki* [2013], to calculate the geoid heights and gravity. For simplicity, we omitted the self-gravitational term, because we are mostly interested in the effects of pPv alone. However, we have checked the effects of self-gravitation for a specific model and confirm that the self-gravitation would not change the results presented in this study.

The density together with a viscosity structure should be defined in the model. We used a model based on the SMEAN seismic tomography data, which uses a weighted average of three different tomography models [*Becker and Boschi*, 2002], to derive the input density. For comparison, we also tested the most recent seismic tomography model, S40RTS [*Ritsema et al.*, 2011]. To obtain a density distribution from a model of seismic anomalies, we used the depth-dependent, shear wave velocity to density scaling factor (see Figure S1a in the supporting information) according to *Steinberger and Calderwood* [2006]. We used a radial viscosity profile consisting of five layers [cf. *Hager and Clayton*, 1989] corresponding to the lithosphere, asthenosphere, upper mantle, transition zone, and lower mantle (see Figure S1b in the supporting information, solid blue line). In addition, in a few cases, we tested the effect of a thermal boundary layer (TBL) by introducing a low-viscosity layer at the bottom of the mantle (see Figure S1b in the supporting information, dashed red line).

The deviation from layered viscosity was formulated using an Arrhenius-type, temperature-dependent viscosity law as follows [cf. *Tackley*, 2000]:

$$\eta(T) = \exp \left[\frac{23.03}{T + T_{\text{ref}}} - \frac{23.03}{2T_{\text{ref}}} \right] \quad (4)$$

where T_{ref} is the nondimensional reference temperature, ($T_{\text{ref}} = 0.5$), and η_0 is the reference viscosity corresponding to the dimensional value of 10^{21} Pa \cdot s. T is the nondimensional temperature, which was obtained as the sum of the nondimensional reference temperature and the perturbation temperature (δT) derived by considering the depth-dependent scaling factor ($S = d \ln \rho / d \ln v_s$) in the following equation:

$$T = T_{\text{ref}} - \frac{d \ln v_s}{\Delta T \alpha} \cdot S \quad (5)$$

$\longleftrightarrow \delta T \longleftrightarrow$

The nondimensional activation energy (23.03) corresponds to a dimensional value for MgSiO₃ perovskite, which is approximately 287 kJ/mol [*Yamazaki and Karato*, 2001] (see Table S1 in the supporting information for all the parameters).

This Newtonian temperature-dependent viscosity is assumed for the lower and upper mantle and leads to an LVV of 0.5 orders of magnitude in the lower mantle and 1.5 orders of magnitude in the upper mantle and forms an immobile lid near the surface. In order to concentrate on the lowermost part of the mantle and the effects of pPv on the geoid, we did not include LVVs associated with weak plate boundaries, which can also be important [e.g., *Kaban et al.*, 2014; *Yoshida and Nakakuki*, 2009].

The postperovskite regions were defined by assigning any point within a depth interval between 2560 km and the CMB having a density anomaly > 0 (i.e., all high S wave anomaly and cold regions), whereas regions with a negative density anomaly were assumed to represent perovskite. In the pPv regions, a modified viscosity was assumed by lowering the temperature-dependent viscosity by a constant factor. These pPv regions characterized by a lower viscosity are clearly visible in Figure 1c as the brownish-red regions bounded by a sharp gradient. Additionally, a pv to pPv density increase of 1.5 to 3.0% was applied to this region (see Figure 1a, blue region).

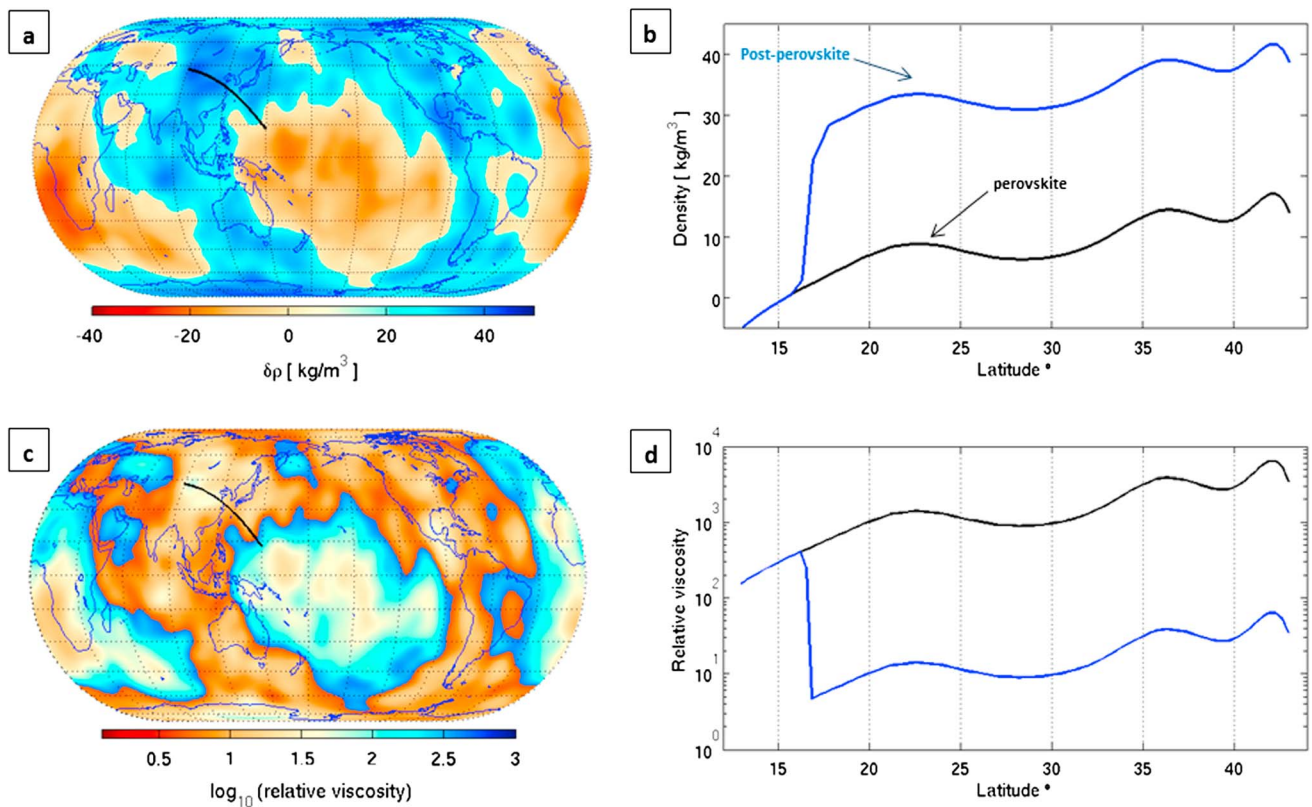


Figure 1. Examples of (a) density anomaly distribution, (c) the lateral viscosity variation, and (b and d) their corresponding cross sections over the western Pacific margin at a depth of 2867 km for the SMEAN seismic tomography model [Becker and Boschi, 2002]. The black and blue profiles show the density (Figure 1b) and lateral viscosity variations (Figure 1d) for the case with perovskite (pv) and postperovskite (pPv), respectively. The jumps in Figures 1b and 1d denote the postperovskite region in which density increased by 1.5% and viscosity decreased by 2 orders of magnitude.

In order to evaluate the fit between the predicted and observed geoid, we used a function referring to variance reduction as follows:

$$VR = \left(1 - \frac{\sum_{n=0}^{n_{\max}} \sum_{m=0}^n (N_{nm}^{\text{predicted}} - N_{nm}^{\text{observed}})^2}{\sum_{n=0}^{n_{\max}} \sum_{m=0}^n (N_{nm}^{\text{observed}})^2} \right) \times 100 \quad (6)$$

where N_{nm}^{observed} and $N_{nm}^{\text{predicted}}$ are the observed and modeled geoid coefficients of degree n and order m , respectively. The maximum degree $n_{\max} = 31$ is chosen based on the resolution of the SMEAN seismic tomography model.

We measured the variance reduction of the model (predicted) geoid with respect to the observed nonhydrostatic geoid up to spherical harmonic degrees of 30 ($n = 2 - 30$). The nonhydrostatic geoid calculated by using the new hydrostatic reference values computed by Chambat *et al.* [2010] and a recent global geopotential model of GOCO015 [Pail *et al.*, 2010], which is a combined satellite gravity field model derived from GOCE and GRACE.

3. Results

As the occurrence of pPv is only associated with relatively cold regions of the lowermost mantle [e.g., Hernlund *et al.*, 2005], only subduction zones are affected. Therefore, we focused on the geoid and its components along a cross section that cuts roughly perpendicular to the western Pacific subduction zones.

3.1. Effects of Low Viscosity and High Density

We first evaluated the geoid for density structure based on the SMEAN, which has been found to outperform other older models in geodynamic applications [Steinberger and Calderwood, 2006]. The lateral viscosity

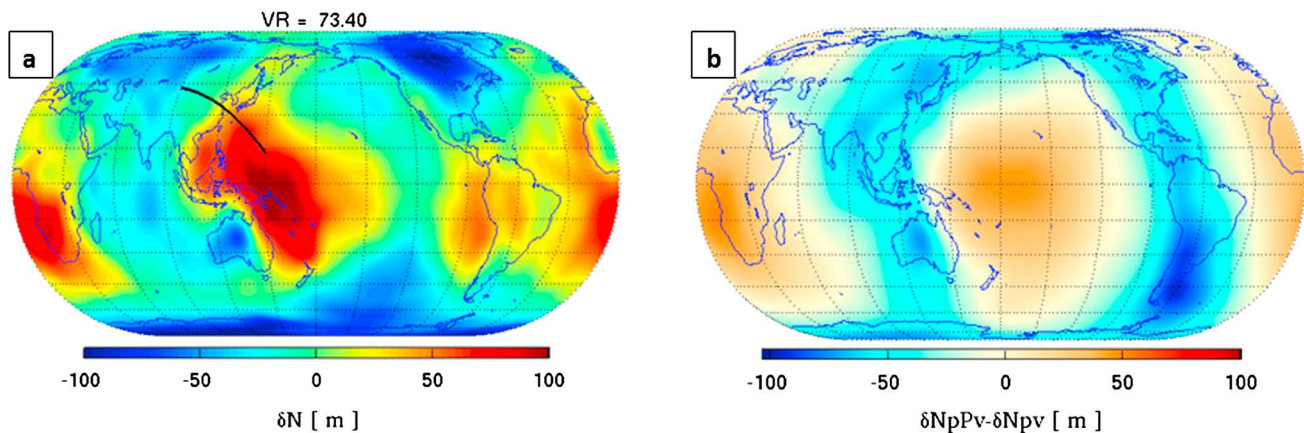


Figure 2. (a) Dynamic geoid and the variance reduction computed for the model based on SMEAN with the postperovskite (pPv), which has a 3 orders of magnitude lower viscosity and 1.5% higher density than the perovskite. (b) The difference between dynamic geoids obtained for model with and without pPv. The lateral viscosity variations in both models (with and without pPv) are obtained from the Arrhenius law.

variations were obtained by assuming a temperature-dependent viscosity for the entire mantle but without considering pPv in the D'' layer.

Subsequently, we assumed the effect of pPv in our models by modifying the viscosity and density within the cold regions (high shear wave velocity) of the D'' layer. In Figure 1a, the blue regions represent the pPv, whereas Figure 1b depicts the locally increased density (blue curve) along the specified profile. The corresponding decrease in the viscosity is shown in Figures 1c and 1d.

Figure 2a shows the geoid heights of the model with pPv in the D'' layer, and Figure 2b depicts the difference between the models with and without pPv. Although the global patterns of the geoid with and without pPv in the D'' layer show a modest difference, their local amplitudes differ significantly from one another. The largest deviations occur around the Pacific, where the low viscous pPv imposed. These variations significantly improve the fit to the observed geoid so that the variance reduction increases from 22.85 to 73.40% by considering weaker and weaker pPv (see Figure S2 in the supporting information).

Focusing on the specific profile, the observed geoid and predicted geoid for model without the presence of pPv are plotted in thick gray and black lines, respectively (Figure 3a). The geoid calculated for the model with LVV due to the presence of pPv (Figure 3a, blue line) shows a drastic reduction for a small decrease in the viscosity, because the low-viscosity region beneath the stiff slabs allows the slab to sink and laterally spread more easily near the bottom. This effect produces a surface dynamic topography with higher (negative) amplitudes, opposite that of the CMB. These results are consistent with the 2-D results of *Tosi et al.* [2009b], who found that the phase transformation from pv to pPv, if accompanied by a decrease in viscosity, considerably reduces the geoid heights over the subduction zones.

A subsequent reduction of the pPv viscosity from 1 to 2 and then from 2 to 3 orders of magnitude decreases the geoid by approximately the same amounts (Figure 3a, blue to red and then red to green). However, a further decrease in the viscosity from 3 to 4 orders of magnitude in the pPv region has a decreasing effect on the geoid amplitude (Figure 3a, green to brown). These results indicate that after applying a viscosity contrast of at least 3 orders of magnitude, the slab resistance forces near the bottom of the downgoing slabs are greatly diminished, and any further increase in the viscosity contrast does not affect the geoid any further (see also Figure S2 in the supporting information).

Figures 3b and 3c show the surface and CMB topography contributions of the different models to the total geoid. The presence of pPv leads to an increase in the negative amplitude of the surface dynamic topography and its contribution to the geoid (Figure 3b, black to blue curve). By contrast, when including the weak pPv, the amplitude of the (negative) dynamic topography at the CMB decreases, and consequently, the negative amplitude of the geoid due to the CMB topography decreases with the

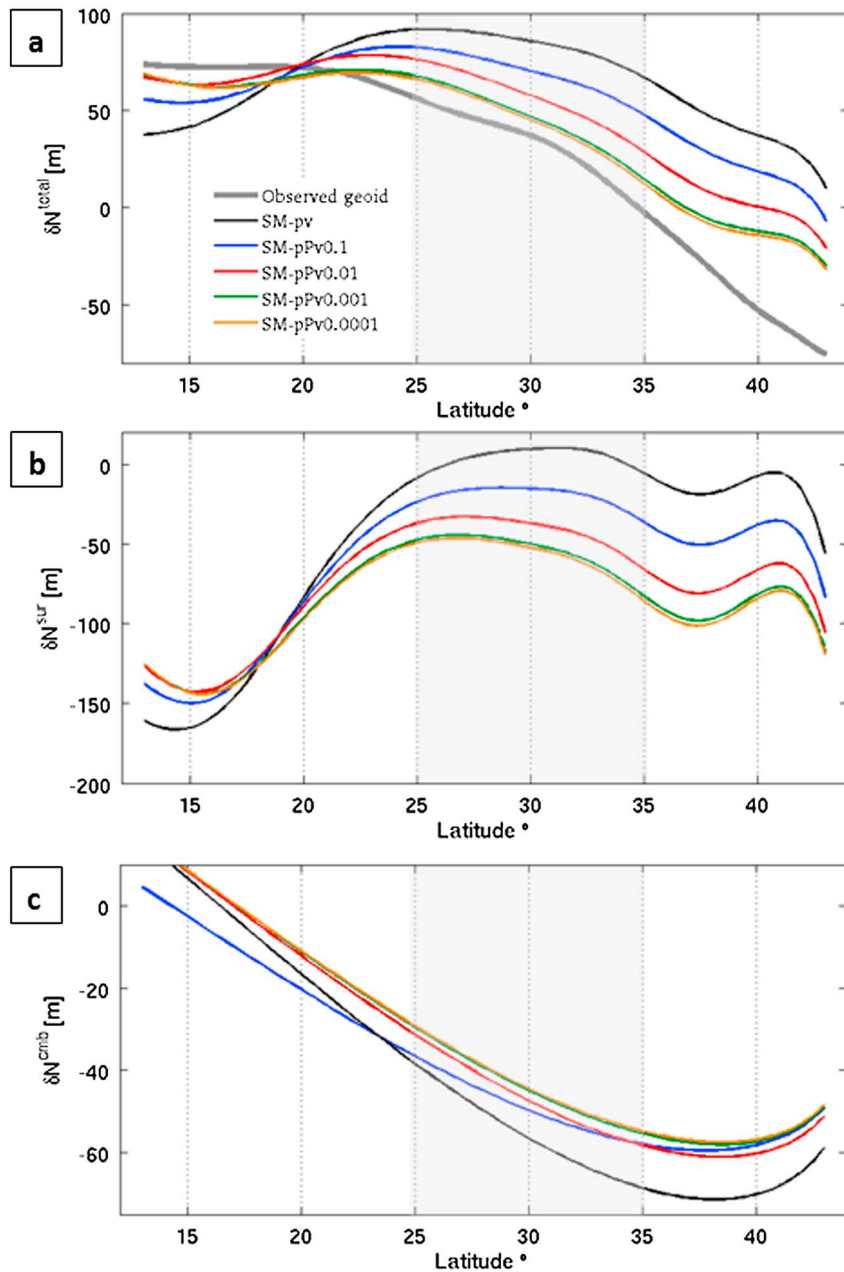


Figure 3. Cross section of (a) observed geoid (thick gray line) for the western Pacific profile and dynamic geoid computed for the perovskite (black) and post perovskite models as function of colatitude. The postperovskite models characterized by 1.5% density increase and a lower viscosity of 1 (blue), 2 (red), 3 (green), and 4 (brown) orders of magnitude. (b and c) The corresponding surface and CMB dynamic topography contributions to the geoid. The shadow boxes roughly indicate the top of subduction plate with 5° each side.

inclusion of pPv. However, this effect is small compared with the surface topography because of the greater distance to the surface (Figure 3c, black to blue curve). Overall, the amplitudes of the topography contributions become closer to the amplitude of the temperature contribution (density anomalies), which has the opposite sign. Consequently, the total geoid above the subduction zones is reduced.

A further weakening of the viscosity yields a smaller (negative) CMB topography and higher (negative) surface topography. However, as mentioned above, after applying a viscosity contrast of at least 3 orders of magnitude, any further increase in the viscosity contrast does not affect the geoid.

3.2. Dependence on Different Tomography Models

As mentioned above, the density anomalies and viscosity variations in the mantle, which are used in various calculations, are defined based on seismic velocities. Many tomography models have been published in recent years. To test the sensitivity of our results to different input models, we also employed the S40RTS model [Ritsema *et al.*, 2011]. The viscosity model was constructed in the same manner as described in section 2, except that the SMEAN model was replaced by S40RTS tomography data.

The global geoid based on the SMEAN tomography provided a better fit compared with that obtained using S40RTS. Thus, the variance reduction of all models is smaller than in the previous models (see Figure S2 in the supporting information). Nevertheless, along the same profile as that studied previously, we achieved a slightly better fit to the observed geoid (see Figure S3 in the supporting information). The effects of pPv are also evident in the S40RTS model because pPv causes a reduction of the geoid high from 68 m in the model without pPv to 53 m, 39 m, and 30 m over the specific profile of western pacific subduction zones when the pPv region is weakened by 1, 2, and 3 orders of magnitude, respectively (see Figure S3 in the supporting information).

3.3. Dependence on the Presence of the Low-Viscosity TBL

Although the strong increase in viscosity with depth from the upper to lower mantle is a common feature of all well-fitting gravity inversion models, the decrease in the viscosity at the base of the mantle as well as its magnitude are poorly defined. Here we tested a model that includes the low-viscosity layer at the base of the mantle covering the entire D'' layer (Figure S1b in the supporting information, red profile). The decreased viscosity in this layer might be related to the effects of the lower TBL [Steinberger and Calderwood, 2006]. Considering this profile already gives a good fit to the observed geoid, so that a variance reduction of 60% is obtained. On top of that, a weak pPv viscosity in the cold area of the D'' layer and LVVs in the overlying mantle are introduced. Indeed, the simultaneous consideration of the TBL and weak pPv in the D'' layer leads to an extreme viscosity reduction which has been reported by Nakada and Karato [2012], based on the decay of the Chandler wobble and tidal deformation of the Earth.

It turns out that the global fit to the observed geoid degraded by 16% in the variance reduction because of a significant decrease in the geoid above the subduction zones. This reduction of the geoid heights is clearly visible over the specific profile of western pacific margin, where a much lower geoid than the observed geoid is obtained (see Figure S4 in the supporting information, dashed red line in comparison with the solid red line). This result provides evidence that the strong viscosity reduction in the lowermost mantle, which has been addressed earlier using gravity inversion models, is partly caused by the presence of weak pPv in this region. Therefore, combining the use of a seismic analysis technique to estimate the pPv distribution in the D'' layer with the inversion methods, it is possible to determine a better viscosity structure.

3.4. Strong Versus Weak pPv

In contrast to the conventional view of the viscosity decrease associated with the presence of pPv in the lower mantle, recent studies [e.g., Karato, 2011] suggest an increased viscosity in the pPv region. We tested this hypothesis by introducing both high-density and high-viscosity pPv into the D'' layer.

The global fit to the observed geoid significantly degraded. The geoid amplitudes are changed considerably, especially over the subduction zones, where the geoid heights became more pronounced (see Figure S5 in the supporting information, dashed red curve). The presence of the strong pPv prevents the bottom of the slab from flowing and spreading easily. Consequently, the amplitude of the negative surface topography is reduced. By contrast, the amplitude of the anomaly due to the CMB is enhanced. Thus, the geoid heights are increased, and the global correlation with the observed geoid is decreased.

3.5. Dependence on the Density Variations

The laboratory and theoretical predictions of the pPv properties suggest a small (1.5%) increase in density associated with a transition from pv to pPv [e.g., Hirose, 2006]. However, our knowledge regarding the pPv phase transition is far from robust, as discussed by Yamazaki and Karato [2013]. Therefore, we performed the same set of tests with a stronger increase (2% and 3%) in density to test the effects of potential density variations on the results presented above. The effects of various density contrasts in combination with different values of the viscosity reductions assumed for the pPv regions are consistent with the findings of

the previous models with a small increase (1.5%) in density. The effect of the pPv-related density is much smaller than the effect of the viscosity. Nevertheless, compared with previous models, a slightly better fit to the observed geoid is achieved. Consequently, the variance reduction of 70% in the case of 1.5% density increase, slightly improved to 71.5 and 74% for a 2 and 3% density increase, respectively (Figure S6 in the supporting information, red to dashed blue and dashed black lines). This improvement is due to increases in both the surface and CMB dynamic topography.

3.6. Dependence on the LVVs in the Whole Mantle

Thus far, we have introduced the LVVs in the D'' layer together with the LVVs in the overlying lower mantle. To focus our attention only on the LVVs in the D'' layer, we performed a calculation that omits the LVVs in the mantle.

Similar to the results of the previous models with a highly viscous slab, the geoid due to the CMB contribution decreases, and the geoid due to the surface topography is enhanced. However, the amplitudes of these variations are much larger than in the presence of LVVs in the lower mantle. Consequently, the geoid is modified, and a better fit to the observed geoid in the specific profile of the western pacific is obtained (see Figure S7a in the supporting information, green compared with blue curve). However, this decrease of geoid height is along with the degrading of the global fit, because the amplitude of geoid decreases relatively in all regions (Figure S7b in the supporting information). In general, our results are consistent with those of previous studies [Moresi and Gurnis, 1996; Zhong and Davies, 1999] reporting that a significant effect on the geoid over high-viscosity slabs depends on whether deep slabs are connected or not connected to top surface. Nevertheless, note that the effect of LVVs in the mantle is strongly dependent on the stratified viscosity profile [Shahraki, 2013], which must be considered in studies endeavoring to find the best fit to the observed geoid.

4. Conclusions

The geoid is highly sensitive to the presence of pPv in the D'' layer. Weak pPv reduces the dynamic topography of the CMB and enhances the amplitude of the surface dynamic topography, which yields a decrease in the geoid above the subduction zones and provides a better fit to the observed geoid. Although the global geoid from SMEAN tomography is dissimilar to that from S40RTS, the effect of pPv is evident in both models. Indeed, the presence of pPv in the lowermost mantle beneath the slabs causes a drastic reduction in the geoid heights over the subduction zones. In comparison with weak pPv, the geoid fit to the observed one is degraded by strong pPv, and the geoid height, especially over the subduction zones, becomes more pronounced.

Considering the model with the lower TBL (2 orders of magnitude), the added presence of pPv in the D'' layer leads to a strong reduction in the viscosity (~4 orders of magnitude). Such strong viscosity reduction within D'' layer has already been inferred from the decay of the Chandler wobble and tidal deformation of the Earth [Nakada and Karato, 2012]. However, our model suggests that the geoid fit degrades for a very strong viscosity reduction due to both a TBL and a weak pPv. Yet the global geoid can be fitted equally well by models without LVVs if a smaller viscosity contrast between lower mantle and CMB is taken into account. Here we believe, from the physical point of view, that it is more realistic to have LVVs in the D'' region and mantle above. Hence, we prefer those models with pPv and LVVs in the mantle. Finally, we found that the presence of LVVs in the lower mantle reduces the effects of weak pPv. This finding implies that inaccurate results may be obtained when considering only pPv in the absence of LVVs in the overlying mantle.

Acknowledgments

We thank Masaki Yoshida for providing the mantle convection code (ConvGS). This work was supported by a grant from the priority research program SPP 1256 of the German Research Foundation (DFG). All calculations were performed at the Center for Scientific Computing of Goethe University, Frankfurt. Data supporting Figure 3 are available as supporting information.

The Editor thanks two anonymous reviewers for their assistance in evaluating this paper.

References

- Ammann, M. W., J. P. Brodholt, J. Wookey, and D. P. Dobson (2010), First-principle constraints on diffusion in lower-mantle minerals and a weak D'' layer, *Nature*, 465(7297), 462–465.
- Becker, T. W., and L. Boschi (2002), A comparison of tomographic and geodynamic mantle models, *Geochem. Geophys. Geosyst.*, 3(1), 1003, doi:10.1029/2001GC000168.
- Cadek, O., and L. Fleitout (2003), Effect of lateral viscosity variations in the top 300 km on the geoid and dynamic topography, *Geophys. J. Int.*, 152(3), 566–580.
- Cadek, O., and L. Fleitout (2006), Effect of lateral viscosity variations in the core-mantle boundary region on predictions of the long-wavelength geoid, *Stud. Geophys. Geod.*, 50(2), 217–232.
- Chambat, F., Y. Ricard, and B. Valette (2010), Flattening of the Earth: Further from hydrostaticity than previously estimated, *Geophys. J. Int.*, 183(2), 727–732.

- Cizkova, H., O. Cadek, C. Matyska, and D. A. Yuen (2010), Implications of post-perovskite transport properties for core-mantle dynamics, *Phys. Earth Planet. Inter.*, *180*(3–4), 235–243.
- Ghosh, A., T. W. Becker, and S. J. Zhong (2010), Effects of lateral viscosity variations on the geoid, *Geophys. Res. Lett.*, *37*, L01301, doi:10.1029/2009GL040426.
- Hager, B. H., and R. W. Clayton (1989), Constraints on the structure of mantle convection using seismic observations, flow models, and the geoid, in *Mantle Convection: Plate Tectonics and Global Dynamics*, edited by R. W. Peltier, pp. 657–763, Gordon and Breach Science Publishers, New York.
- Hernlund, J. W. (2013), Deep Earth: Mantle fabric unravelled?, *Nat. Geosci.*, *6*(7), 516–518.
- Hernlund, J. W., C. Thomas, and P. J. Tackley (2005), A doubling of the post-perovskite phase boundary and structure of the Earth's lowermost mantle, *Nature*, *434*(7035), 882–886.
- Hirose, K. (2006), Postperovskite phase transition and its geophysical implications, *Rev. Geophys.*, *44*, RG3001, doi:10.1029/2005RG000186.
- Hunt, S. A., D. J. Weidner, L. Li, L. P. Wang, N. P. Walte, J. P. Brodholt, and D. P. Dobson (2009), Weakening of calcium iridate during its transformation from perovskite to post-perovskite, *Nat. Geosci.*, *2*(11), 794–797.
- Kaban, M. K., I. Rogozhina, and V. Trubitsyn (2007), Importance of lateral viscosity variations in the whole mantle for modelling of the dynamic geoid and surface velocities, *J. Geodyn.*, *43*(2), 262–273.
- Kaban, M. K., A. G. Petrunin, H. Schmeling, and M. Shahraki (2014), Effect of decoupling of lithospheric plates on the observed geoid, *Surv. Geophys.*, *35*, 1361–1373.
- Karato, S. I. (2010), The influence of anisotropic diffusion on the high-temperature creep of a polycrystalline aggregate, *Phys. Earth Planet. Inter.*, *183*(3–4), 468–472.
- Karato, S. I. (2011), Rheological structure of the mantle of a super-Earth: Some insights from mineral physics, *Icarus*, *212*(1), 14–23.
- Kido, M., and O. Cadek (1997), Inferences of viscosity from the oceanic geoid: Indication of a low viscosity zone below the 660-km discontinuity, *Earth Planet. Sci. Lett.*, *151*(3–4), 125–137.
- Moresi, L., and M. Gurnis (1996), Constraints on the lateral strength of slabs from three-dimensional dynamic flow models, *Earth Planet. Sci. Lett.*, *138*(1–4), 15–28.
- Moucha, R., A. M. Forte, J. X. Mitrovica, and A. Daradich (2007), Lateral variations in mantle rheology: Implications for convection related surface observables and inferred viscosity models, *Geophys. J. Int.*, *169*(1), 113–135.
- Murakami, M., K. Hirose, K. Kawamura, N. Sata, and Y. Ohishi (2004), Post-perovskite phase transition in MgSiO₃, *Science*, *304*(5672), 855–858.
- Nakada, M., and S. Karato (2012), Low viscosity of the bottom of the Earth's mantle inferred from the analysis of Chandler wobble and tidal deformation, *Phys. Earth Planet. Inter.*, *192*, 68–80.
- Nakagawa, T., and P. J. Tackley (2011), Effects of low-viscosity post-perovskite on thermo-chemical mantle convection in a 3-D spherical shell, *Geophys. Res. Lett.*, *38*, L04309, doi:10.1029/2010GL046494.
- Nowacki, A., J. Wookey, and J. M. Kendall (2010), Deformation of the lowermost mantle from seismic anisotropy, *Nature*, *467*(7319), 1091–1095.
- Oganov, A. R., and S. Ono (2004), Theoretical and experimental evidence for a post-perovskite phase of MgSiO₃ in Earth's D'' layer, *Nature*, *430*(6998), 445–448.
- Ohta, K., S. Onoda, K. Hirose, R. Sinmyo, K. Shimizu, N. Sata, Y. Ohishi, and A. Yasuhara (2008), The electrical conductivity of post-perovskite in Earth's D'' layer, *Science*, *320*(5872), 89–91.
- Pail, R., et al. (2010), Combined satellite gravity field model GOCO01S derived from GOCE and GRACE, *Geophys. Res. Lett.*, *37*, L20314, doi:10.1029/2010GL044906.
- Ricard, Y., L. Fleitout, and C. Froidevaux (1984), Geoid heights and lithospheric stresses for a dynamic Earth, *Ann. Geophys.*, *2*(3), 267–286.
- Ricard, Y., M. Richards, C. Lithgowbertelloni, and Y. Lestunff (1993), A geodynamic model of mantle density heterogeneity, *J. Geophys. Res.*, *98*(B12), 21,895–21,909, doi:10.1029/93JB02216.
- Richards, M. A., and B. H. Hager (1984), Geoid anomalies in a dynamic Earth, *J. Geophys. Res.*, *89*(B7), 5987–6002, doi:10.1029/JB089iB07p05987.
- Richards, M. A., and B. H. Hager (1989), Effects of lateral viscosity variations on long-wavelength geoid anomalies and topography, *J. Geophys. Res.*, *94*(B8), 10,299–10,313, doi:10.1029/JB094iB08p10299.
- Ritsema, J., A. Deuss, H. J. van Heijst, and J. H. Woodhouse (2011), S40RTS: A degree-40 shear-velocity model for the mantle from new Rayleigh wave dispersion, teleseismic traveltimes and normal-mode splitting function measurements, *Geophys. J. Int.*, *184*(3), 1223–1236.
- Shahraki, M. (2013), *Dynamics of Mantle Circulation and Convection: The Signatures in the Satellite Derived Gravity Fields*, 218 pp., Frankfurt Univ., Germany.
- Shim, S. H., T. S. Duffy, R. Jeanloz, and G. Shen (2004), Stability and crystal structure of MgSiO₃ perovskite to the core-mantle boundary, *Geophys. Res. Lett.*, *31*, L10603, doi:10.1029/2004GL019639.
- Steinberger, B., and A. R. Calderwood (2006), Models of large-scale viscous flow in the Earth's mantle with constraints from mineral physics and surface observations, *Geophys. J. Int.*, *167*(3), 1461–1481.
- Tackley, P. J. (2000), Self-consistent generation of tectonic plates in time dependent, three-dimensional mantle convection simulations. Part 1: Pseudoplastic yielding, *Geochem. Geophys. Geosyst.*, *1*(1), 1021, doi:10.1029/2000GC000036.
- Tosi, N., O. Cadek, and Z. Martinec (2009a), Subducted slabs and lateral viscosity variations: Effects on the long-wavelength geoid, *Geophys. J. Int.*, *179*(2), 813–826.
- Tosi, N., O. Cadek, Z. Martinec, D. A. Yuen, and G. Kaufmann (2009b), Is the long-wavelength geoid sensitive to the presence of postperovskite above the core-mantle boundary?, *Geophys. Res. Lett.*, *36*, L05303, doi:10.1029/2008GL036902.
- Tsuchiya, T., J. Tsuchiya, K. Umemoto, and R. A. Wentzcovitch (2004), Phase transition in MgSiO₃ perovskite in the Earth's lower mantle, *Earth Planet. Sci. Lett.*, *224*(3–4), 241–248.
- Yamazaki, D., and S.-I. Karato (2001), Some mineral physics constraints on the rheology and geothermal structure of Earth's lower mantle, *Am. Mineral.*, *86*(4), 385–391.
- Yamazaki, D., and S.-I. Karato (2013), Lattice-preferred orientation of lower mantle materials and seismic anisotropy in the D'' layer, in *Post-Perovskite: The Last Mantle Phase Transition*, edited by K. Hirose et al., pp. 69–78, AGU, Washington, D. C.
- Yoshida, M. (2008), Core-mantle boundary topography estimated from numerical simulations of instantaneous mantle flow, *Geochem. Geophys. Geosyst.*, *9*, Q07002, doi:10.1029/2008GC002008.
- Yoshida, M., and A. Kageyama (2004), Application of the Yin-Yang grid to a thermal convection of a Boussinesq fluid with infinite Prandtl number in a three-dimensional spherical shell, *Geophys. Res. Lett.*, *31*, L12609, doi:10.1029/2004GL019970.
- Yoshida, M., and T. Nakakuki (2009), Effects on the long-wavelength geoid anomaly of lateral viscosity variations caused by stiff subducting slabs, weak plate margins and lower mantle rheology, *Phys. Earth Planet. Inter.*, *172*(3–4), 278–288.
- Zhang, S. X., and U. Christensen (1993), Some effects of lateral viscosity variations on geoid and surface velocities induced by density anomalies in the mantle, *Geophys. J. Int.*, *114*(3), 531–547.
- Zhong, S. J., and G. F. Davies (1999), Effects of plate and slab viscosities on the geoid, *Earth Planet. Sci. Lett.*, *170*(4), 487–496.